Materials Advances

ROYAL SOCIETY OF CHEMISTRY

PAPER

View Article Online
View Journal | View Issue

Cite this: *Mater. Adv.*, 2026, 7, 1678

Reline-assisted synthesis of fcc-hcp Ni/Ni(OH)$_2$ nanocatalyst for effective reductive hydrogenation of 4-nitrophenol

Md. Minhajul Alam Khan, [a] Shawon Saha, [a] Sumaya Nur Mithila,[a] Yeasin Arafat Tarek, [b] Akter Hossain Reaz [c] and Shakhawat H. Firoz *[a]

This study presents a facile, eco-friendly, and controlled reline-assisted chemical reduction method to synthesize fcc-hcp Ni/Ni(OH)$_2$ nanocomposites. The conventional chemical reduction process was modified by replacing water with reline to produce the Ni/Ni(OH)$_2$ nanocomposite (Ni-reline). The incorporation of precursor salt in reline significantly influenced its physicochemical properties. Specifically, the optimized concentration of nickel salt in reline (0.4 mol dm^{-3}) reduced its viscosity from 573 cP to 57 cP and increased its conductivity, which played a crucial role in the nucleation and growth of nanoparticles. As a consequence, coral reef-like nanostructures (~39 nm) developed in reline, whereas in aqueous media, spherical Ni nanoparticles (Ni-Aq.) with a significantly larger particle size (~92 nm) were formed. Elemental analysis further confirmed the presence of carbon in Ni-reline, derived from the DES matrix. Ni-Aq. and Ni-reline were evaluated as catalysts for the reductive hydrogenation of 4-nitrophenol to 4-aminophenol. Ni-reline exhibited superior catalytic activity, achieving 95% conversion in 20 minutes with a rate constant of 0.1336 min^{-1}, 11 times higher than Ni-Aq. This enhancement is attributed to the mixed-phase structure, increased surface area, and surface-bound carbon species promoting adsorption and electron transfer. Moreover, Ni-reline demonstrated excellent reusability over five consecutive cycles due to easy magnetic separation with minimal catalyst loss. This study highlights the potential of reline to modify nanostructure growth and phase behavior for efficient, environmentally friendly catalytic applications.

Received 3rd November 2025,
Accepted 30th December 2025

DOI: 10.1039/d5ma01275a

rsc.li/materials-advances

1. Introduction

Rapid industrialization has resulted in increased environmental pollution, especially water contamination, emerging as a critical threat to human health and the ecosystem.[1] Despite global awareness, industrial activities continue to discharge hazardous pollutants, especially in developing countries.[2,3] Among the diverse pollutants affecting water bodies, nitrophenol and its derivatives are one of the most detrimental contaminants. These compounds are released during the production of synthetic dyes, medicines, pesticides, herbicides, and insecticides.[4] The high toxicity of nitrophenols, particularly their potential to cause severe damage to human organs such as the kidney, liver, and central nervous system, has led to their classification as one of the "worst 114 organic contaminants" by the United States Environmental Protection Agency (USEPA).[5] Given the risks associated with nitrophenol, it is crucial to find effective methods for its degradation or removal, as well as to explore opportunities for converting it into value-added chemical products. Hence, various remediation techniques have already been explored, including oxidation,[6] microbial degradation,[7] electrochemical removal,[8] adsorption,[9] and catalytic hydrogenation.[10,11]

Among these, catalytic hydrogenation is remarkable due to its cost-effectiveness, high efficiency, and conversion ability of nitrophenols into less toxic aromatic amines.[12–14] Metal nanoparticles (NPs), especially noble metals such as gold, silver, platinum, and palladium, have exhibited exceptional catalytic performance in the reduction of 4-NP.[4,15] Although noble metals exhibit excellent catalytic activity, their limited availability and high cost severely limit their wider use, leading to a search for suitable catalysts that are abundant and cost-effective.[16] Thus, transition metal nanoparticles (TMNPs) appear to be a viable alternative to noble metals in the role as catalysts. Among them, nickel nanoparticles show promise due to their cost, easy reusability, and good catalytic activity.[17,18]

[a] *Department of Chemistry, Bangladesh University of Engineering and Technology (BUET), Dhaka-1000, Bangladesh. E-mail: shfiroz@chem.buet.ac.bd*
[b] *School of Mechanical and Mining Engineering, The University of Queensland, St Lucia, Queensland 4072, Australia*
[c] *Department of Chemistry, Michigan State University, East Lansing, MI 48824, USA*

However, developing Ni NPs with enhanced catalytic properties is hindered by their intrinsic instability. The magnetic dipole interactions in Ni NPs and strong van der Waals forces tend to promote the agglomeration of NPs, which is detrimental in reducing the active surface area and inducing some unwanted phase transitions.[19,20] This may compromise the structural integrity of the NP, leading to a decrease in its catalytic efficiency. As a result, in order to alleviate Ni NP limitations, attempts to improve their catalytic characteristics have emerged as a primary focus.

Catalytic properties of a catalyst are intrinsically related to its shape and particle size, as these factors have a direct impact on surface area, active site distribution, and electronic structure.[21] For example, Wang *et al.*[22] synthesized Ni NPs with chemical modifiers like citric acid and CTAB and tested their catalytic activity in the hydrogenation of 4-NP to 4-AP. The citric acid-modified Ni NPs showed increased catalytic activity due to their smaller particle size and improved dispersion properties. While Darband *et al.*[23] used Ni nanocones as a very efficient and stable catalyst for the electrochemical hydrogen evolution reaction. Aside from size and shape, phase structure can provide additional flexibility for modulating the catalytic performance of desired materials because different crystal phases have different spatial atomic arrangements and coordination status, which can affect substrate adsorption or activation and product desorption.[24,25] For instance, Zhang *et al.*[26] examined the hydrogenation of nitrophenols using unsupported Ni nanocrystals with fcc and hcp phases. The hcp-phase Ni nanocrystals showed superior catalytic activity and selectivity, because of their enhanced surface energy and higher active site concentration.

In addition, Yang *et al.*[27] synthesized a Ni catalyst with both hcp and fcc crystal phases, demonstrating remarkable catalytic hydrogenation efficacy across a wide range of substrates, including nitro compounds, aldehydes, ketones, alkenes, and nitrogen-containing heterocycles. It is expected that the mixed crystal phase exerts a synergistic effect, considerably increasing the catalyst's intrinsic activity. However, phase stability remains a concern, as metastable domains may relax over time, diminishing catalytic efficiency.[28] Ni exhibits two allotropes: stable fcc and metastable hcp. The hcp phase is less energetically favorable and typically requires external stabilization.[29] In contrast, $Ni(OH)_2$ in its hcp crystal is well stable, and the hcp-phase $Ni(OH)_2$ provides strong adsorption sites for reaction intermediates and facilitates proton-coupled electron transfer, ultimately enhancing catalytic properties.[30,31] So, $Ni/Ni(OH)_2$ in fcc-hcp mixed phase with controlled morphology has high potential to perform as a prominent catalyst for 4-NP reduction.

However, controlled synthesis of NPs often requires adding stabilizers or capping agents to control particle size and prevent aggregation.[32] For instance, Sidhaye *et al.*[33] utilized sodium dodecyl sulfate and oleic acid as surfactants and capping agents to regulate the growth of Ni NPs. Xu *et al.*[34] achieved a uniform, monomorphic, self-assembled flower-like Ni microstructure using polyvinylpyrrolidone. Kim *et al.*[35] synthesized ultrafine Ni powders in the presence of sodium carboxymethyl cellulose, while Nandi *et al.*[36] prepared Ni using sulfonated polybutadiene. But these additives often contain long-chain hydrocarbons or synthetic polymers that are harmful and toxic, and may cause environmental contamination.[37] Hence, there is a growing interest in developing alternatives to conventional stabilizers or capping agents that will be environmentally friendly and enable precise control over NPs growth.

In search for alternatives to conventional stabilizers or capping agents, deep eutectic solvents (DESs), a class of green solvents, have emerged. DESs are formed by the combination of hydrogen bond acceptors (HBAs) and hydrogen bond donors (HBDs), resulting in stable liquids with unique and tunable physicochemical properties. It has gained significant attention, particularly in the field of NPs synthesis, due to its ability to regulate NPs nucleation and growth by stabilizing surface charges, modulating reduction potentials, and altering chemical activities.[38] For example, Gomes-Junior *et al.*[39] reported ultra-small CeO_2 NPs ($\sim$0.73 nm) with controlled spherical morphology in reline DES, where reline governed reaction kinetics and stabilized nascent surfaces. In related work, Datta *et al.*[40] showed that reline facilitates Au NP formation by (i) acting as a mild reducing environment *via* ammonia released from urea hydrolysis and (ii) tuning gold-precursor speciation to stabilize Au^+ and suppress rapid disproportionation, thereby enabling controlled reduction. So, DES is now an established system for controlling the growth dynamics of NPs, particularly reline, a eutectic mixture of choline chloride and urea in 1 : 2 molar ratios with a melting point between 12 °C and 24 °C, which is significantly lower than their individual melting point,[41] has been widely studied. Because of its supramolecular structure and strong hydrogen-bonding network, reline can act as both a solvent medium and a stabilizing agent, effectively controlling NP shape and size.[42,43] This dual role is particularly advantageous for developing NPs with unique surface characteristics and specific properties essential for catalytic applications.[44,45] Given reline's ability to control the size of particles, morphology, and even phase structure, using reline as a growth medium in chemical reduction methods presents a promising, environmentally friendly strategy for synthesizing $Ni/Ni(OH)_2$ nanocomposite hydrogenation catalysts with increased activity and selectivity. However, the significance of reline in NP morphology and phase structure optimization, notably in Ni NPs, remains unclear.

Herein, this study focuses on developing of a simple chemical reduction approach for synthesizing fcc-hcp $Ni/Ni(OH)_2$ mixed-phase nanocomposite with reline as the growth medium. Unique properties of reline allow for the formation of a mixed crystal phase and precise control over composite shape. In addition, the physicochemical features of reline are investigated in the controlled production of the $Ni/Ni(OH)_2$ nanocomposite. This fcc-hcp $Ni/Ni(OH)_2$ nanocomposite is then used as a hydrogenation catalyst to reduce 4-NP, with performance comparable to that of fcc Ni.

2 Experimental

2.1 Materials

Nickel chloride hexahydrate ($NiCl_2{\cdot}6H_2O$; Sigma-Aldrich, Germany), sodium hydroxide pellets (NaOH; Sigma-Aldrich, Germany), hydrazine hydrate 99% ($N_2H_4{\cdot}H_2O$; Sigma-Aldrich, Germany), choline chloride ($C_5H_{14}ClNO$; TCI, Japan), urea crystal ($CO(NH_2)_2$; Merck, Germany), sodium borohydride ($NaBH_4$; Sigma-Aldrich, Germany) and 4-nitrophenol ($C_6H_5NO_3$; Merck, Germany) were procured from commercial sources and utilized directly without any further purification. Deionized water (approximately 0.66 μS cm^{-1}) was utilized for preparing the solutions in the experiment. The DI water was obtained from a from a DI-water purification system (Barnstead NanoPure, Thermo Fisher Scientific, USA).

2.2 Synthesis of materials

2.2.1 Synthesis of reline. Reline was synthesized by utilizing choline chloride (ChCl) as the hydrogen bond acceptor (HBA) and urea as the hydrogen bond donor (HBD), following the established protocol as reported previously.[46] Before the preparation, ChCl was heated to 90 °C for 2 hours in a vacuum oven to eliminate any moisture content. The reline was obtained by mixing ChCl and urea with a molar ratio of 1 : 2, heating and stirring the mixture at 80 °C for 2 hours, resulting in a transparent liquid. Subsequently, the formed DES was cooled to room temperature, tightly sealed, and stored under ambient conditions.

2.2.2 Synthesis of Ni/Ni(OH)$_2$ nanocomposite. Ni NPs were synthesized in aqueous medium (denoted as Ni-Aq.) using the chemical reduction method, following the procedure described in an earlier report.[47] This approach is simply optimized by replacing the aqueous medium with the reline to prepare Ni/$Ni(OH)_2$ nanocomposite (Ni-reline). To prepare the Ni-reline, 0.135 mol of $NiCl_2{\cdot}6H_2O$ was dissolved in 37.5 mL of reline DES, followed by the addition of 0.45 mol of $N_2H_4{\cdot}H_2O$ into a 100 mL round-bottom flask under vigorous stirring. Initially, a pale violet gel was formed, and then the flask's wall was rinsed with approximately 5–10 mL of reline. As the reaction proceeded, a Ni complex formed between Ni^{2+} ions and hydrazine, and then 30 mL of NaOH solution (50%) was added. Then the reaction was stirred continuously for 1 hour, during which the final black precipitate of Ni-reline was formed. The product was washed thoroughly with deionized water and ethanol, then dried at 40 °C in a hot air oven for 24 hours. The Schematic representation of the synthesis of Ni-reline is illustrated in Fig. 1.

2.3 Characterization

The surface morphology with elemental composition of the synthesized samples was characterized using a field emission scanning electron microscopy (FESEM, model JSM-7600F, JEOL, Japan) integrated with energy dispersive X-ray spectroscopy (EDS). Phase identification and crystallinity were examined through X-ray diffraction (XRD) analysis using a Smartlab diffractometer (Rigaku, Japan). Functional groups present in the nanoparticles were determined *via* Fourier transform infrared (FTIR) spectroscopy, with spectra collected in transmission mode over the range of 4000–400 cm^{-1} using an FTIR-8400 spectrophotometer (Shimadzu, Japan). Surface chemical composition was further analyzed by X-ray photoelectron spectroscopy (XPS) employing a Kratos AXIS Nova system (Kyoto, Japan) equipped with a monochromatic Al Kα source (photon energy = 1486.6 eV).

2.4 Surface charge analysis

The surface charge characteristics of the material were assessed using the point of zero charge (PZC) method, which identifies the pH at which the net surface charge becomes neutral under controlled conditions of temperature, pressure, and ionic strength.[48,49] For this analysis, 0.2 g of the sample was suspended in 40 mL of 0.1 M $NaNO_3$ solution within 50 mL centrifuge tubes. The pH of each suspension was adjusted to target values of 2, 4, 6, 7, 8, 10, and 12 (±0.1) using 0.1 M NaOH. Before initiating the agitation process, the initial pH (pH_i) of the supernatants was measured. Next, the tubes were placed on an orbital shaker (Stuart-SSL1) and shaken for 24 hours at 200 rpm. After settling, each supernatant's final pH (pH_f) was determined, and to calculate the PZC, the pH change ($\Delta pH = pH_i - pH_f$) was plotted against the initial pH. To ensure consistency, the operation was performed again with a 0.05 M

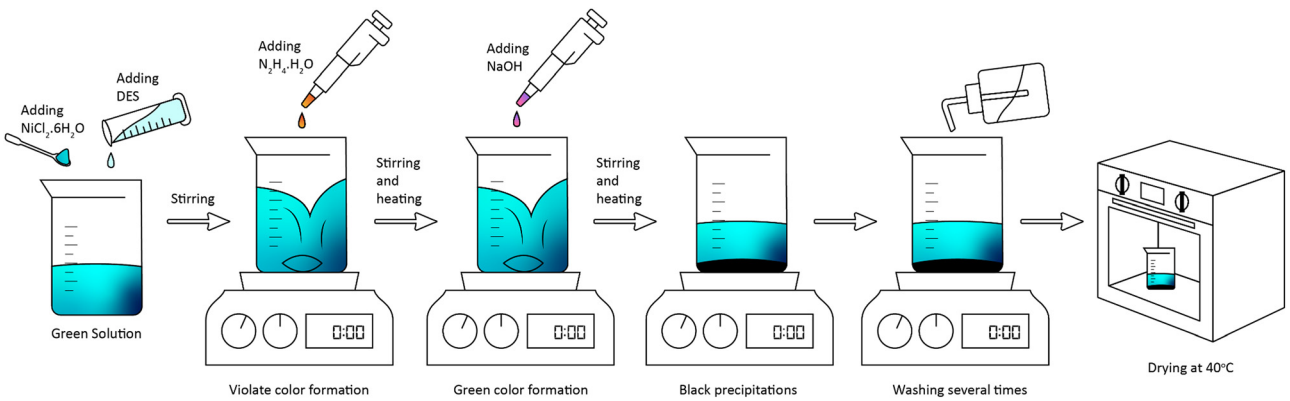

Fig. 1 Schematic representation of the synthesis of Ni-reline.

$NaNO_3$ solution. All measurements were carried out in triplicate, and the mean result was used for further analysis.

2.5 Investigation of the catalytic activity in the reductive hydrogenation of 4-NP

The catalytic properties of Ni-Aq. and Ni-reline was investigated in the reductive hydrogenation of 4-NP to 4-AP through a UV-vis spectroscopic method. To confirm the presence of 4-NP, a 1 mM solution (300 μL) was added to 6 mL of DI water, and the absorbance at 317 nm was measured. While, in the absence of a catalyst, mixing $NaBH_4$ (10 mM, 1 mL) with the 4-NP solution resulted in an immediate color shift to a bright yellow, indicating the formation of phenolate ions, as detected at 400 nm by UV-vis spectroscopy. Then, catalytic tests involved adding 1 mL of a 5 mg mL^{-1} nanocatalyst suspension to the mixture of 4-NP, $NaBH_4$, and water, with reaction progress tracked *via* absorbance decrease at 400 nm until complete reduction. Effects of pH (pH 3 to pH 11) and catalyst dosage (3 to 5 mg mL^{-1}) on reduction efficiency were investigated. Catalyst stability and reusability were assessed over multiple cycles by magnetic separation, washing, and reused without drying.

3 Results and discussion

3.1 Characterization

The surface characteristics and morphology of the synthesized materials were analyzed in greater detail using field emission scanning electron microscopy (FESEM), as shown in Fig. 2. Fig. 2(a) and (b) display the FESEM images of Ni-Aq. at low and high magnifications, respectively, while Fig. 2(c) and (d) present the FESEM images of Ni-reline at low and high magnifications, respectively. In Fig. 2(a) and (b), it is observed that monodispersed Ni nanospheres were formed with an average particle size of ~92 nm, while Fig. 2(c) and (d) depicts that Ni-reline possessed a coral reef like morphology, with an average particle size of ~39 nm, which is smaller than Ni-Aq., and other than particle size, the nanostructure developed high porosity and surface defects. A comparative histogram of particle size distribution for both samples is provided in Fig. S1. These results demonstrated a notable difference in both morphology and particle size between the Ni-Aq. and Ni-reline. This variation is attributed to the distinct physicochemical properties of the reline system, which affect the nucleation and growth dynamics of the nanoparticles.[50]

Additionally, the elemental composition of Ni-reline was analyzed using energy dispersive X-ray spectroscopy (EDS), as shown in Fig. 2(e). The EDS spectrum of Ni-reline exhibited prominent peaks at 0.525 keV and 0.851 keV, corresponding to the K-shell of oxygen (O) and the L-shell of nickel (Ni), respectively. The O content was found to be 15.68%, while the Ni content was 68.13%. These findings suggest the possibility of Ni oxide or hydroxide being present, in addition to metallic Ni. Moreover, two distinct peaks at 0.277 keV and 0.392 keV were observed, which are attributed to the K-shell of carbon (C) and nitrogen (N), likely originating from the reline counterparts. Based on these observations, it is indicative of the possible formation of a $Ni/Ni(OH)_2$ nanocomposite, enriched with carbon content.

Furthermore, the crystalline structure and phase purity of the synthesized materials were analyzed using X-ray diffraction (XRD) as depicted in Fig. 3(a). Fig. 3(a(i)) represents Ni-Aq. (blue line), displayed three distinct peaks at 2θ = 44.5°, 51.8°, and 76.4°, which correspond to the (111), (200), and (220) planes of pure face-centered cubic (fcc) Ni (JCPDS card: 96-900-9863).[51] As no additional peaks were present, this indicated the purity of the synthesized Ni NPs in the aqueous system. In contrast, Fig. 3(a(ii)) represents Ni-reline (red line) showcasing new peaks at 33.4°, 38.5°, and 59.3° denoted by (*), corresponding to the (100), (10$\bar{1}$) and (110) planes referred to the formation of β-$Ni(OH)_2$ with brucite type hexagonal close-packed (hcp)

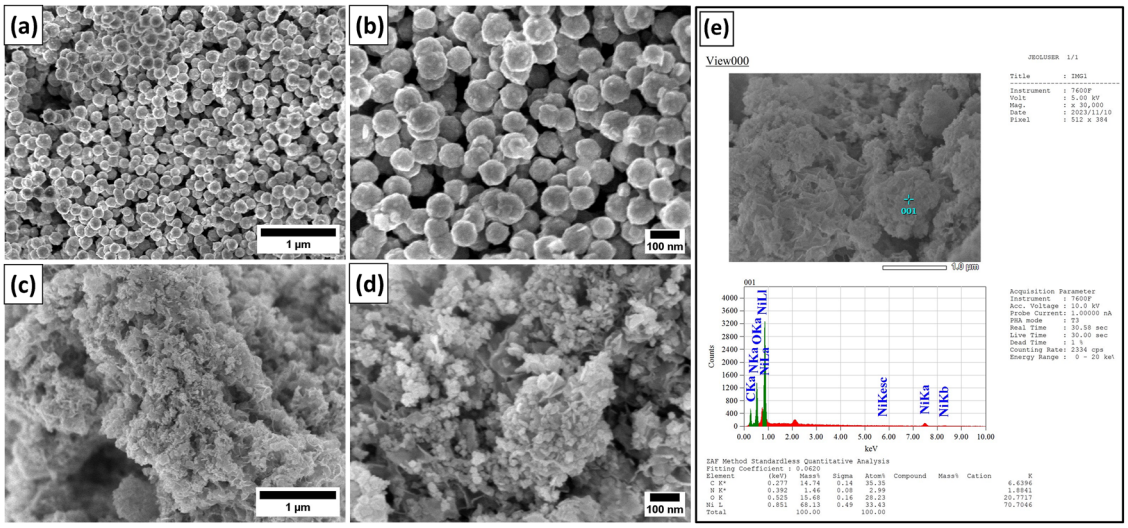

Fig. 2 FESEM images of (a) Ni-Aq. (at low magnification), (b) Ni-Aq. (at high magnification) (c) Ni-reline (at low magnification) (d) Ni-reline (at high magnification) and (e) EDS spectra of Ni-reline.

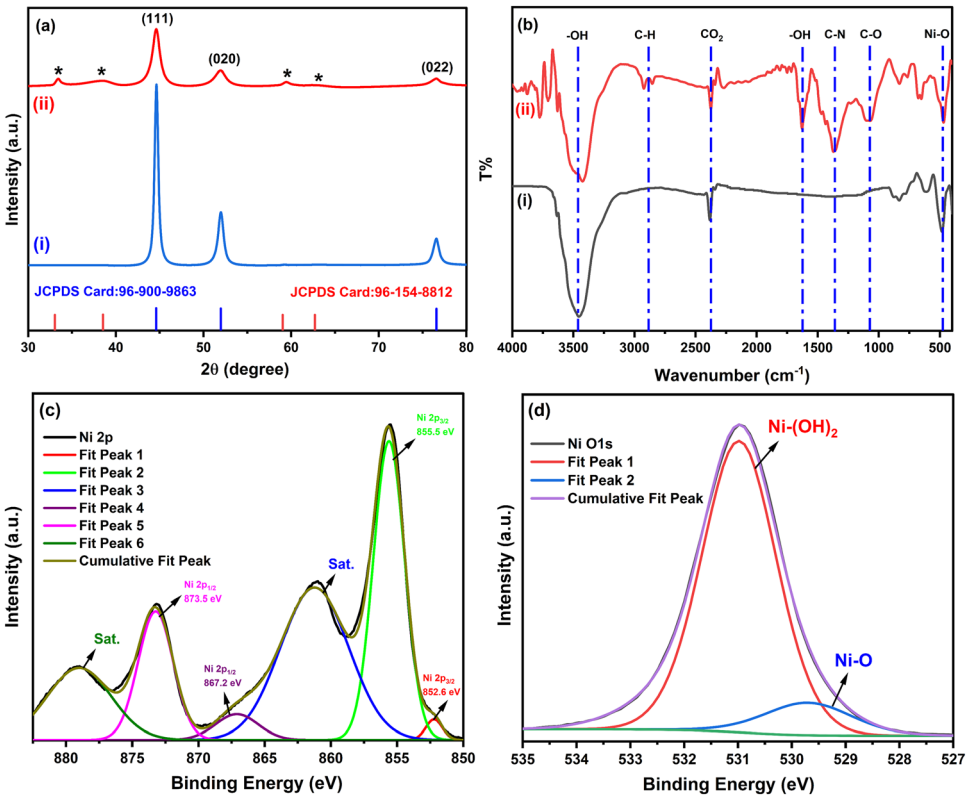

Fig. 3 (a) XRD spectra of (i) Ni-Aq. and (ii) Ni-reline, (b) FTIR spectra of (i) Ni-Aq. and (ii) Ni-reline, and High-resolution XPS spectra of (c) Ni 2p and (d) O 1s for Ni-reline.

crystal system (JCPDS card: 96-154-8812), along with the characteristic fcc Ni peaks.[52] The presence of both fcc and hcp phases suggested that the Ni-reline sample comprises a mixed crystal system and confirmed the formation of a Ni/Ni(OH)$_2$ nanocomposite.

Moreover, the XRD spectrum indicated that Ni-reline exhibited broad peaks with decreasing intensity compared to Ni-Aq., suggesting that Ni-reline possessed lower crystallinity and smaller crystallite size. Ni-Aq. remained in a highly crystalline state with 98% crystallinity, while the crystallinity of Ni-reline decreased to 80%. The decrease in crystallinity was likely due to the presence of the highly viscous reline system, which inhibited crystal growth and disrupted the reduction process, ultimately leading to the formation of a new crystal system of hcp Ni(OH)$_2$. The average crystallite size of Ni-Aq. and Ni-reline was found to be 16 nm and 7 nm, respectively, as calculated from the significant diffraction peaks using the Debye–Scherrer equation, as shown in eqn (1).[53]

$$D = \frac{k\lambda}{\beta \cos\theta} \quad (1)$$

To further investigate the surface functional group present on the synthesized materials, Fourier transform infrared (FTIR) spectroscopy was performed. The corresponding FTIR spectra for Ni-Aq. and Ni-reline are shown in Fig. 3(b). In Fig. 3(b), distinctive peaks in the 400–650 cm^{-1} range, corresponding to Ni–O stretching vibrations, confirmed the formation of Ni in both samples.[54] A band around 2200–2300 cm^{-1} was attributed to the stretching modes of CO_2 absorbed from the air,[55] while the broad peak at 3400–3600 cm^{-1} indicated –OH vibrations, suggesting hydrogen bonding and water absorption.[56] In Ni-reline, additional peaks were observed, including those at 1000–1100 cm^{-1} (νC–O and νC–N vibrations), 1347 cm^{-1} (C–N stretching),[57,58] and a band around 1630 cm^{-1}, likely originating from the vibrations of the C=O bond (carbonyl group from urea), as well as an N–H vibration band, possibly due to ammonia formation during urea hydrolysis.[59] The peak around 2800–3000 cm^{-1} corresponded to C–H stretching vibrations, linked to the alkyl chains in the DES structure, suggesting that carbon contents were present on the surface of the materials, originating from the adsorption of DES components.[60] Therefore, the FTIR analysis suggested that carbon and nitrogen contents were likely present on the materials' surface, which correlated with the observations from the EDS analysis.

To further confirm the presence of Ni(OH)$_2$ and metallic Ni in the Ni-reline, X-ray Photoelectron Spectroscopy (XPS) was performed. In Fig. 3(c), two distinct peaks at 873.5 eV and 855.5 eV corresponded to the Ni 2p$_{1/2}$ and Ni 2p$_{3/2}$ spin–orbit components of Ni(OH)$_2$, respectively. These peaks were further accompanied by two satellite (sat.) peaks, which were associated with the Ni 2p$_{1/2}$ and Ni 2p$_{3/2}$ peaks. Upon deconvolution of the spectrum, additional signals at 867.2 eV and 852.6 eV were identified, which corresponded to the Ni 2p$_{1/2}$ and Ni 2p$_{3/2}$ binding energies of metallic Ni, indicating the presence of

metallic Ni alongside $Ni(OH)_2$. Further investigation of the O 1s spectra, displayed in Fig. 3(d), located a strong peak at 531.5 eV, indicating the existence of $Ni(OH)_2$. In addition, a weaker signal at 529.5 eV revealed the presence of NiO with lower content. Furthermore, the XPS survey spectrum (Fig. S2(a)) revealed the presence of Ni, O, C, and N, with elemental composition information provided in Table S1. On top of that, the C 1s and N 1s XPS spectra, displayed in Fig. S2(b) and (c), confirmed the existence of C and N in the sample, which were obtained during synthesis. The C 1s spectra revealed peaks corresponding to C=O and C–C bonds, obtained from DES counterparts and the N 1s spectra also verified the existence of primary amine groups that are produced from the urea molecules. Thus, the XPS analysis established the formation of a Ni/$Ni(OH)_2$ nanocomposite in the reline system, as evidenced by the presence of characteristic peaks for $Ni(OH)_2$ and metallic Ni, along with the presence of C and N components from the reline system during the synthesis process.

3.2 Possible mechanism for DES-mediated Ni/$Ni(OH)_2$ formation

In the present study, metallic Ni NP was obtained from the aqueous system, while in the reline system, Ni/$Ni(OH)_2$ nanocomposite was formed. This obvious distinction emphasizes the unique function of reline in controlling nanoparticle growth dynamics. DESs play a significant role in nucleation and growth processes by neutralizing charges, modulating reduction potentials, changing chemical actions, altering crystal facets, and directing growth along distinct crystallographic directions.[61,62] The distinctive physicochemical features and complex framework of DESs lead to nanomaterial growth dynamics that are markedly different from those of conventional aqueous systems.

In aqueous media, as hydrazine hydrate was introduced to the $NiCl_2$ solution, a stable Ni complex formed instantly. Upon addition of NaOH, this complex dissociated, resulting in the formation of $Ni(OH)_2$ *via* the sol–gel process.[63] Afterwards, $Ni(OH)_2$ was reduced by excess N_2H_4, resulting in the recrystallization of monodispersed spherical Ni NPs. The readily produced Ni complex acts as a protective matrix during particle formation, which prevents new particles from aggregating. Consequently, uncontrolled agglomeration was avoided during nucleation and growth, resulting in monodisperse spherical NPs. The reaction scheme of the formation of Ni NPs in an aqueous system is shown here as described by Choi *et al.*[47]

Step 1: Formation of pale violate gel

$$NiCl_{2(aq.)} + 3N_2H_{4(aq.)} \rightarrow [Ni(N_2H_4)_3Cl_2]_{(thick\ gel)}$$

Step 2: Stabilization of complex

$$[Ni(N_2H_4)_3]Cl_2 \rightarrow [Ni(N_2H_4)_2]Cl_2 + N_2H_4$$

$$[Ni(N_2H_4)_3]Cl_2 + 5/2N_2H_4 \rightarrow [Ni(NH_3)_6]Cl_2 + 3/2N_2$$

Step 3: Ligand exchange *via* introducing OH^- to form Ni NPs

$$Ni^{2+} + N_2H_4 + OH^- \rightarrow 2Ni + N_2 + 4H_2O$$

In contrast, in reline, Ni/$Ni(OH)_2$ nanocomposite was formed, which exhibited different size and shape than the Ni prepared in aqueous media. This difference resulted from reline's distinct physicochemical properties like viscosity and conductivity, which differed greatly from those of the aqueous media. Because these features had a significant impact on the reduction rate and growth kinetics during nanoparticle formation, comprehending the physicochemical behavior of the reline was important in determining the mechanisms behind Ni/$Ni(OH)_2$ formation.

Reline possesses a considerably greater viscosity than most commonly used DES systems.[64] The increased viscosity in reline was caused by the effect of urea as a hydrogen bond donor (HBD). Urea's strong hydrogen bonding characteristic assisted in the formation of a substantial and dense hydrogen bonding network with ChCl, effectively reducing the average free volume or void size within the solvent matrix.[65] The ensuing structural compactness and reduced molecular mobility directly led to the reline system's enhanced viscosity.[66] Interestingly, the incorporation of $NiCl_2$ salt (Ni^{2+} ion) into the reline system resulted in a sudden decrease in viscosity, deviating from the conventional behavior found in most molecular solvents, where solute addition typically increases viscosity by promoting liquid structuring. As shown in Fig. 4(a), the addition of Ni^{2+} ions to an aqueous system resulted in a modest increase in viscosity, which is consistent with usual solvent–solute interactions. Conversely, the addition of Ni^{2+} ions significantly decreased the viscosity of the reline system, with a minimum of 0.4 mol dm^{-3} of Ni^{2+} ions. This drop in viscosity can be ascribed to the disruption of the reline system's native hydrogen bonding network. Such disruption effectively increases the average void size in the solvent matrix and facilitates enhancing molecular mobility and mass transport.[67] In addition to the viscosity trends, Fig. 4(b) shows that the electrical conductivity of the reline system increased with Ni^{2+} ion concentration. The decreased viscosity with elevated metal ion concentrations enabled increased ion mobility, which improved overall mass transport throughout the system. All together, these results indicate that the reline's physicochemical properties were very sensitive to precursor concentration, which affected the system's viscosity and conductivity.

The native robust hydrogen bonding of the reline system was rapidly disrupted with the incorporation of Ni^{2+}, resulting in the release of urea molecules. Additionally, the hygroscopic nature of pure reline, which contained trace amounts of water, led to the hydrolysis of the free urea molecules, resulting in the formation of ammonia.[40]

$$NH_2CONH_2 + H_2O \rightarrow 2NH_3 + CO_2$$

Ammonia exhibits reducing potential since it has lone pair electrons on the nitrogen atom that can be shared, making it a well-known reducing agent, as earlier reported in the synthesis of different NPs such as ZnO, $CoFe_2O_4$, and Ag.[68] Consequently, the reduction process of Ni^{2+} in reline diverged significantly from that in aqueous media, principally due to the presence of ammonia. This mechanistic differential promotes the

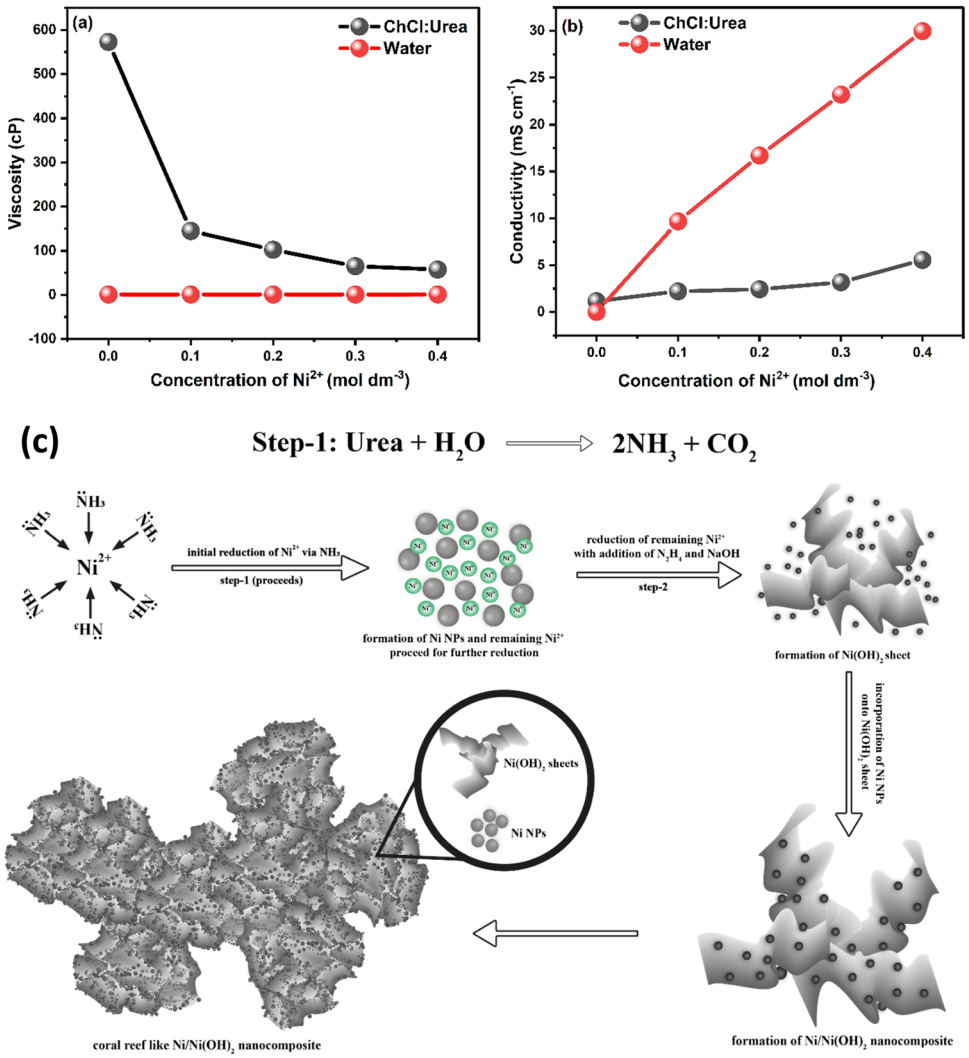

Fig. 4 Effect of Ni^{2+} concentration on (a) viscosity, (b) conductivity of aqueous and reline systems and (c) schematic illustration of the $Ni/Ni(OH)_2$ formation in reline system.

formation of $Ni/Ni(OH)_2$ in the reline system. The formation of $Ni/Ni(OH)_2$ in reline could be attributed to a two-step reduction process:

(i) Step 1: The hydrogen bonding network of reline was disrupted, causing the generation of ammonia, which served as an agile reducing agent, aiding the reduction of Ni^{2+} ions to metallic Ni NPs. Initially, Ni^{2+} remains in high concentrations that facilitate fast nucleation of Ni NPs. Though there was a drop in viscosity as precursor salt was incorporated, the solvent's viscosity remained high enough to impede ionic mobility, resulting in partial reduction of some Ni^{2+} ions.

(ii) Step 2: The remaining unreacted Ni^{2+} ions formed a stable coordination complex with the hydrazine hydrate. Following the addition of NaOH, this compound underwent ligand exchange to decompose the Ni complex into $Ni(OH)_2$. The excess hydrazine present in aqueous media could further decrease $Ni(OH)_2$, however, in reline, the high viscosity persisted that limited ionic mobility and prevented excess hydrazine from reducing $Ni(OH)_2$. As a consequence, $Ni/Ni(OH)_2$ mixed-phase nanocomposite formed in place of pure metallic Ni. In Ni-reline, XRD analysis revealed that the $Ni(OH)_2$ phase has a brucite-type hcp crystal structure. Each Ni^{2+} ion in this structure was octahedrally coordinated by six OH^- ions, resulting in two-dimensional layers. These layers were tightly connected within the plane but very weakly kept together between planes due to van der Waals forces or hydrogen bonding. This feature facilitated anisotropic growth, culminating in the development of $Ni(OH)_2$ nanosheet.[69] A schematic illustration of the $Ni/Ni(OH)_2$ formation in the reline system is represented in Fig. 4(c).

3.3 Catalytic hydrogenation of 4-NP to 4-AP

The catalytic hydrogenation of 4-NP to 4-AP in the presence of $NaBH_4$ was carried out utilizing Ni-Aq. and Ni reline as hydrogenation catalyst. As shown in Fig. S3(a), UV-vis spectra demonstrated that the 4-NP solution initially exhibited an absorption peak at 317 nm, which shifted to 400 nm upon the addition of $NaBH_4$, indicating the formation of the 4-nitrophenolate ion.

Upon introduction of the catalyst, a new peak at 300 nm appeared, which confirms the formation of 4-AP, while the 400 nm peak gradually decreased, demonstrating the reduction process. In the 4-NP reduction process, $NaBH_4$ can act as the reducing agent by dissociating in aqueous media to form borohydride ions (BH_4^-). These BH_4^- ions are capable of donating hydride ions (H^-), which are essential for the reduction of the nitro group in 4-NP. This reaction is thermodynamically feasible, as the reduction potential of BH_4^- is sufficiently negative to reduce the nitro group into an amine group. However, in the absence of a catalyst, this reaction is kinetically restricted due to the high kinetic barrier caused by the electrostatic repulsion between the negatively charged BH_4^- and the phenolate ion (the deprotonated form of 4-nitrophenol under alkaline conditions).[70] As a result, without a catalyst, the 400 nm peak remained unchanged after 120 minutes, indicating no significant reduction of 4-NP, as shown in Fig. S3(b). This highlights the necessity of a suitable catalyst for efficient reduction. To address this, Ni-Aq. and Ni-reline nanocatalysts were employed in the reduction process. As demonstrated in Fig. S3(c) and (d), Ni-Aq. showed a slow conversion rate, with the 400 nm peak decreasing over 90 minutes without reaching full conversion. In contrast, Ni-reline caused the 400 nm peak to disappear within 20 minutes, demonstrating its superior catalytic efficiency.

A comparative catalytic performance of Ni-Aq. and Ni-reline after 20 minutes, depicted in Fig. 5(a), and UV-vis spectral analysis confirmed that Ni-reline exhibited remarkable catalytic performance in the reductive hydrogenation of 4-NP.

As Ni-reline possessed coral reef like morphology with smaller particle size compared to Ni-Aq., resulting in an increased active surface area for catalysis, additionally, the presence of carbon in Ni-reline enhanced its adsorption capability, which in turn promoted the reduction process. Moreover, the presence of a mixed-phase of Ni-reline (fcc Ni and hcp $Ni(OH)_2$) enhanced electrical properties by developing a synergistic interface that facilitated charge transfer and increased the density of active sites. The coexistence of fcc and hcp phases resulted in different atomic configurations and electronic states, which boosted conductivity by allowing electrons to move more efficiently across phase boundaries. This heterogeneity also modified the local work function and surface potential, promoting faster electron exchange during catalytic reactions.[30,71] So, the enhanced catalytic activity of Ni-reline can be ascribed to the following key features, its reduced particle size, distinct surface properties, and the presence of a mixed-phase crystal structure.

The kinetics of the reactions were considered to follow pseudo-first-order kinetics as there was a significant difference in the concentration of $NaBH_4$ and 4-NP. Furthermore, to

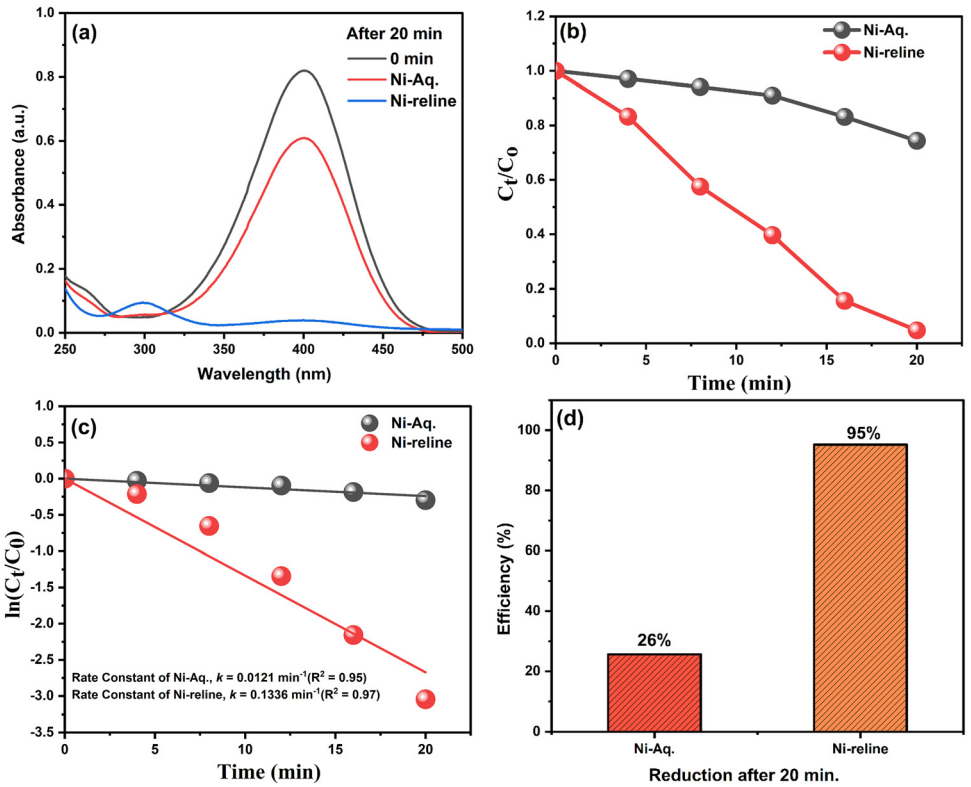

Fig. 5 (a) Comparative UV-vis absorption spectra of catalytic hydrogenation of 4-NP with Ni-Aq. and Ni-reline catalyst after 20 minutes; comparative pseudo-first-order kinetic data for the hydrogenation reaction employed (b) plot (C_t/C_0) *vs.* reaction time, (c) plot $\ln(C_t/C_0)$ *vs.* time and (d) hydrogenation efficiency after 20 minutes. (The reaction conditions included, concentration of 4-NP: 1 mM; concentration of $NaBH_4$: 10 mM; catalyst dosage: 5 mg; temperature: 25 °C).

assess the efficacy of the synthesized nanocatalysts, pseudo-first-order kinetics was applied, as represented in eqn (2).[72]

$$\ln\left(\frac{C_t}{C_0}\right) = \ln\left(\frac{A_t}{A_0}\right) = -k_{app} \quad (2)$$

The value of (C_t/C_0) is equivalent to the relative intensity of absorbance (A_t/A_0), where A_t and A_0 represent the absorbance values at time t and time 0, respectively. Here, Fig. 5(b) represented the change in relative concentration (C_t/C_0) with time for the reduction of 4-NP to 4-AP upon utilizing Ni-Aq., and Ni-reline as catalysts and it was found that the relative absorption intensity of 4-NP by the Ni-reline was the lowest after 20 minutes, referring the best catalytic activity. Moreover, the rate constant of the reaction was measured using $\ln(C_t/C_0)$ *vs.* time plot, as shown in Fig. 5(c). An excellent linear correlation as the regression coefficient, $R^2 \approx 0.96$ was obtained and the value of k was determined from the slope of the linear plot which was found to be 0.0142 min^{-1} and 0.1553 min^{-1} for Ni-Aq. and Ni-reline in the hydrogenation reaction of 4-NP to 4-AP. Fig. 5(d) demonstrated the catalytic efficiency of Ni-Aq. and Ni-reline, was found to be 26% and 95% respectively. So, it highlights that the catalytic efficiency of Ni-reline is way superior than Ni-Aq. sample. Additionally, a comparative summary of the correlation coefficient of $\ln(C_t/C_0)$ *vs.* time plot, rate constant, and percent efficiency for the reduction of 4-NP of the synthesized nanocatalysts is presented in Table S2. Furthermore, effect of catalyst dosage on the effectiveness of Ni-reline was investigated, and catalytic tests were conducted using Ni-reline dosages of 3 mg mL^{-1}, 4 mg mL^{-1}, and 5 mg mL^{-1}. A Comparative analysis demonstrated that a 5 mg mL^{-1} dosage achieved the most efficient reduction of 4-NP over time, as illustrated in Fig. S4(a)–(d). Additionally, Table S3 summarizes the rate constants (k), regression coefficients (R^2), and efficiencies (%) corresponding to each catalyst dosage.

Another important parameter that affects the catalyst's performance is the pH of the reaction media. Hence, the most suitable pH condition for Ni-reline in the catalytic hydrogenation reaction was analyzed. At various pH conditions, the catalytic hydrogenation reaction of 4-NP to 4-Ap by Ni-reline was observed. Fig. 6(a) shows the effect of the solution's pH on the catalytic performance of Ni-reline in the hydrogenation reaction of 4-NP.

It was observed that Ni-reline exhibited superior catalytic activity at pH 3. At pH 3, the catalytic hydrogenation reaction was completed after 12 minutes, reaching equilibrium with an efficiency of 98%. In contrast, at pH 5, the catalytic hydrogenation reaction completed after 16 minutes, reaching equilibrium with an efficiency of 97%. At pH 7, after 20 minutes, the efficiency of Ni-reline was around 95%, but it did not reach equilibrium. On the other hand, as the solution pH increased and solution basicity rose, the efficiency of Ni-reline decreased, as shown in Table S4. Therefore, it could be said that as the pH of the solution decreased and the acidity increased, the catalytic performance of Ni-reline was significantly enhanced. The enhancement in performance was due to the modification in the catalyst surface charge. The catalyst's surface charge varied drastically as the pH of the solution changed, affecting its catalytic efficiency. In catalytic hydrogenation, the effective adsorption of reactant molecules onto the surface of the catalyst is crucial for accelerating the reduction reaction. Modifying the surface charge of the catalyst can significantly influence its adsorption behavior, thereby impacting overall catalytic performance.

Therefore, the surface charge of a material can be investigated using the PZC test, which determines the pH at which the surface charge of components become neutral under controlled conditions of temperature, pressure, and solution composition.[73] The PZC test was conducted on Ni-reline and demonstrated an isoelectric point of 9.01, as shown in Fig. 6(b). Once the pH of the solution is less than PZC, the net surface charge on the solid surface for the adsorbent becomes positive because of the adsorption of excess protons. On the other hand, the net surface charge becomes negative when the pH of the solution is higher than PZC. Hence, Ni-reline remained positively charged in neutral aqueous media due to proton adsorption. It was observed that the reduction rate of 4-NP increased with decreasing solution pH (Fig. 6(a)). When the solution pH was below the PZC, the catalyst surface acquired a net positive charge, which

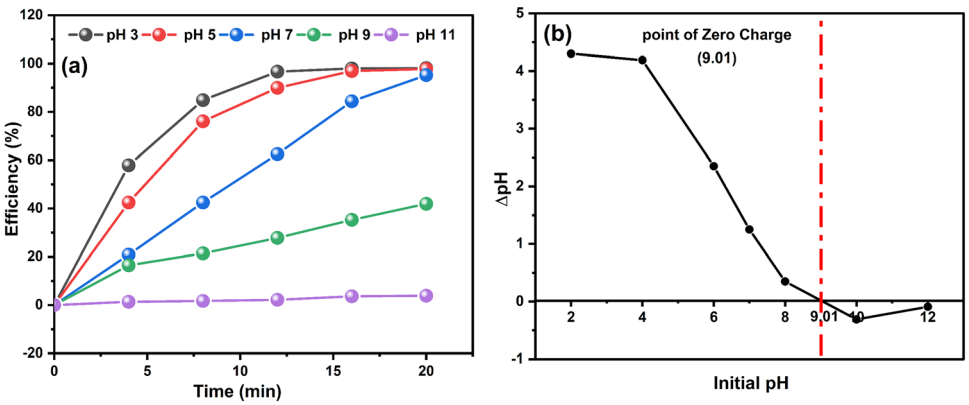

Fig. 6 (a) Effect of solution's pH in catalytic hydrogenation reaction of 4-NP (b) Determination of isoelectric point of Ni-reline (the reaction conditions included, 4-NP concentration: 1 mM; $NaBH_4$ concentration: 10 mM; catalyst dosage: 5 mg; temperature: 25 °C).

enhanced the electrostatic adsorption of the negatively charged nitrophenolate ions. This increased adsorption affinity facilitated a more rapid reduction of nitrophenolate ions by molecular hydrogen.

3.4 A possible mechanism of the catalytic hydrogenation of 4-NP by Ni-reline

Based on the observations described above, a possible mechanism is proposed for the catalytic reduction of 4-NP by Ni-reline and illustrated in Fig. 7. It is anticipated that at the start of the catalytic hydrogenation reaction, the adsorption of the reductant and reactant on the surface of Ni-reline bears the most significance. As a reducing agent, $NaBH_4$ in aqueous medium can react with water at ambient temperature, yielding H_2 and the sodium metaborate ($NaBO_2$) by-product, causing 4-NP to convert into its corresponding 4-nitrophenolate ion that is the reactant.[74] It was observed from the surface charge analysis that in neutral condition, surface of the catalyst remained positive due to the adsorption of the hydronium ion. Consequently, the negatively charged 4-nitrophenolate ions were electrostatically adsorbed onto the positively charged surface of the catalyst. Furthermore, adsorption of nitrophenolate ion significantly improved due to the deposition of carbon on the surface of the Ni-reline from DES media, resulting in a synergistic effect. Previous reports suggested that the presence of carbon content synergistically improves materials' adsorptive properties.[75]

Conversely, in the presence of a catalyst, the newly formed hydrogen molecules dissociate and adsorb onto the metal surface, resulting in the formation of Metal–H species. These Ni-reline-H intermediates initiate the reduction by transferring electrons from the hydride to the catalyst, which are then directed toward the positively charged nitrogen atom in the nitro group of 4-NP. This electron transfer reduces the nitro group to a nitroso intermediate. Subsequent hydrogenation transforms the nitroso molecule into hydroxylamine, which further reduced into the corresponding aniline derivative.[76]

Ni-reline has superior catalytic efficiency than Ni-Aq., owing to its unique mixed-phase structure, which comprises both fcc and hcp crystal systems. These structural characteristics have a substantial impact on the catalyst's electronic properties, contributing to increase its performance. The fcc phase of Ni imparts strong electrical conductivity, allowing for efficient electron transport over the catalyst surface. Meanwhile, the hcp phase of $Ni(OH)_2$ offers structural heterogeneity and interfacial barriers, which improve charge separation and localized electron accumulation.[77] The coexistence of these two crystal systems results in synergistic interfacial interactions that reduce the overall electron flow resistance while shortening charge migration paths. This structural design shifts the reduction potential of Ni, allowing faster electron transport during the hydrogenation process.[78] Furthermore, phase barriers and lattice mismatches between the fcc and hcp domains can cause crystal defects and increase the density of electronic states (DOS) around the Fermi level.[79] These electronic optimizations enhance the material's ability to adsorb and activate hydrogen species, allowing for a faster conversion of 4-NP into 4-AP.

3.6 Reusability of the Ni-reline catalyst

To assess the reusability and stability of the Ni-reline catalyst, it was employed in the catalytic reduction of 4-NP over five

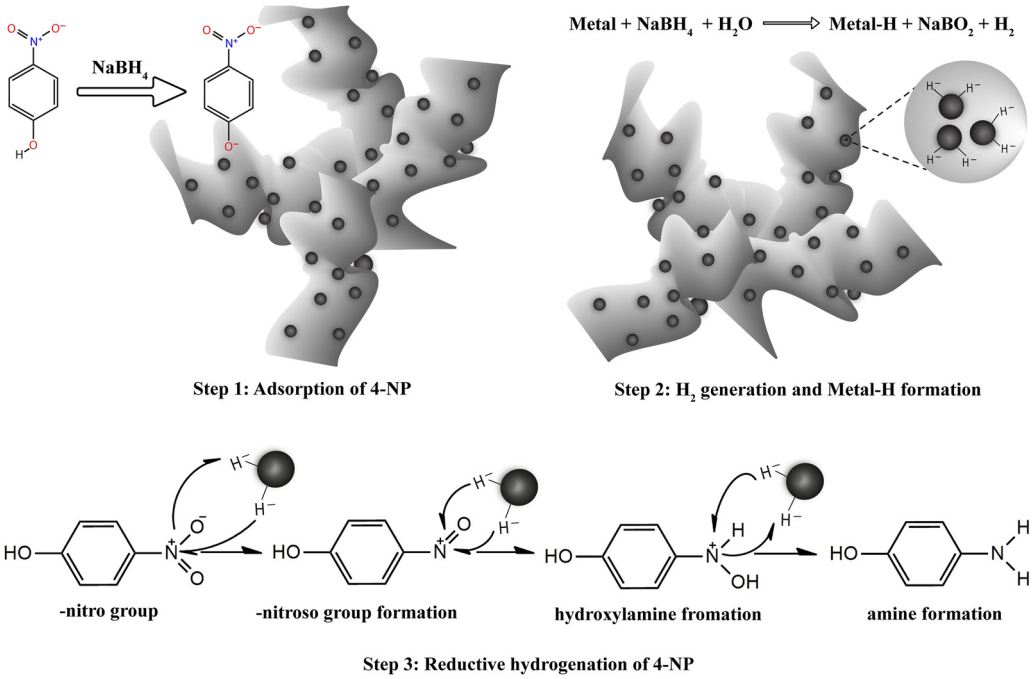

Fig. 7 A possible mechanism for the reduction of 4-NP catalyzed by the Ni-reline.

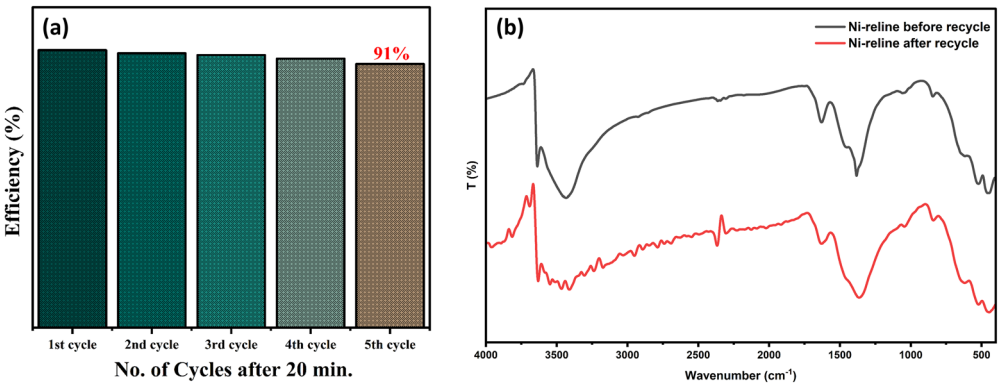

Fig. 8 (a) Analysis of the reusability of Ni-reline in the hydrogenation of 4-NP (b) FTIR spectra of Ni-reline catalyst before and after five consecutive catalytic cycles.

successive reaction cycles. After each reaction cycle, the catalyst was recovered from the reaction mixture, thoroughly rinsed, and then reintroduced under the same experimental conditions for reuse. The catalytic efficiency after each cycle, as shown in Fig. 8(a), demonstrates the catalyst's excellent stability. There is only a marginal decrease in performance, from 95% to 91%, after five repeated catalytic processes. This remarkable retention of performance can be attributed to the well-structured crystal nature and magnetic properties of the Ni-reline catalyst, which allows for easy separation without significant loss of the sample. For clarity, the magnetic separation process of nanocatalyst is schematically represented in Fig. S5.

Furthermore, to evaluate the structural integrity and stability of the Ni-reline catalyst, FTIR spectroscopy was performed for the Ni-reline catalyst before and after being employed in five consecutive catalytic cycles, as shown in Fig. 8(b). The FTIR spectra revealed no significant variations between the two samples. Key peaks observed in the 400–650 cm^{-1} range in both the fresh and recycled catalysts correspond to Ni–O stretching vibrations, confirming the presence of Ni.[53] Additionally, a narrow and strong band at 3634 cm^{-1}, which is characteristic of the O–H stretching vibration of $Ni(OH)_2$,[79] was observed in both samples, suggesting that the $Ni/Ni(OH)_2$ structure remained intact. However, in the recycled Ni-reline catalyst, a slight haziness was observed in the high wavenumber region of the FTIR spectrum. This suggests the presence of carbonaceous residues, despite this, no new peaks were detected, indicating that the catalyst remained structurally stable and retained its integrity for further use.

4. Conclusion

This study demonstrated a strategic and environmentally benign approach for synthesizing $Ni/Ni(OH)_2$ heterostructures with a mixed fcc-hcp crystal system by modulating a conventional chemical reduction method with reline DES. In the conventional aqueous system, metallic Ni with a pure fcc crystal structure was obtained, while replacing the reaction medium with reline resulted in the formation of a $Ni/Ni(OH)_2$ nanocomposite with a mixed fcc-hcp crystal structure. The structural variation observed in the reline system was attributed to the modulation of the physicochemical properties of reline upon the addition of Ni salt. Specifically, the addition of the precursor salt reduced the viscosity of reline from 573 cP to 57 cP while increasing its ionic conductivity. These alterations resulted in a coral reef-like morphology with smaller particles ($\sim$39 nm) in Ni-reline, compared to the spherical morphology with increase particles size ($\sim$92 nm) in the aqueous system (Ni-Aq.). In the reductive hydrogenation of 4-NP, Ni-reline showed a substantially higher rate constant (0.1336 min^{-1}), nearly 11 times greater than Ni-Aq. This improved catalytic activity is caused by the synergistic effects of the mixed-phase structure, abundant surface defects, and increased surface area. Furthermore, elemental analysis confirmed the presence of carbonaceous species in Ni-reline, which improves adsorption, while surface charge analysis revealed a positively charged surface that promotes stronger electrostatic interaction with negatively charged nitrophenolate ions, speeding up the reaction. These findings highlight the versatility of reline as a sustainable solvent capable of regulating nanoparticle phase, shape, and surface chemistry.

Author contributions

Md. Minhajul Alam Khan: conceptualization, methodology, data curation, formal analysis, investigation, visualization, writing – original draft. Shawon Saha: formal analysis, investigation, writing – review and editing. Sumaya Nur Mithila: formal analysis, methodology. Yeasin Arafat Tarek: visualization, writing – review and editing. Akter Hossain Reaz: visualization, writing – review and editing. Shakhawat H. Firoz: conceptualization, project administration, resources, supervision, writing – review and editing.

Conflicts of interest

The authors declare no conflict of interest.

Data availability

The data that is used to support the conclusions of this research may be found inside the article as well as the files that are associated with its supplementary information (SI). Supplementary information is available. See DOI: https://doi.org/10.1039/d5ma01275a. Additional data that support the findings of this study are available from the corresponding author upon reasonable request.

Acknowledgements

The authors would like to acknowledge the laboratory and financial support from Bangladesh University of Engineering & Technology (BUET).

References

1 L. Xiong, Y. Fu, Y. Luo, Y. Wei, Z. Zhang, C. Wu, S. Luo, G. Wang, D. Sawtell and K. Xie, *J. Mater. Res.*, 2022, **37**, 2109–2123.
2 J.-R. Chiou, B.-H. Lai, K.-C. Hsu and D.-H. Chen, *J. Hazard. Mater.*, 2013, **248**, 394–400.
3 N. P. P. Pabbathi, N. M. Nathani, I. R. Gadhvi and M. Chandrashekar, *Environmental Biotechnology*, Springer, 2020, vol. 1, pp. 197–225.
4 X.-X. Yan, Y.-F. Zhang, Y. Chen and B. Wang, *Colloids Surf., A*, 2020, **598**, 124826.
5 S. Balgude, K. Patil, S. Moharil, M. Puranik, S. Kadam, P. Lokhande, S. Patange and P. More, *ChemistrySelect*, 2022, **7**, e202200221.
6 J. D. Donaldson, S. M. Grimes, N. G. Yasri, B. Wheals, J. Parrick and W. E. Errington, *J. Chem. Technol.*, 2002, **77**, 756–760.
7 R. Dai, J. Chen, J. Lin, S. Xiao, S. Chen and Y. Deng, *J. Hazard. Mater.*, 2009, **170**, 141–143.
8 N. Kaur and V. Singh, *New J. Chem.*, 2017, **41**, 2844–2868.
9 E. Marais and T. Nyokong, *J. Hazard. Mater.*, 2008, **152**, 293–301.
10 Z. Wu, J. Chen, Q. Di and M. Zhang, *Catal. Commun.*, 2012, **18**, 55–59.
11 R. K. Narayanan and S. J. Devaki, *Ind. Eng. Chem. Res.*, 2015, **54**, 1197–1203.
12 Y. Shaoqing, H. Jun and W. Jianlong, *Radiat. Phys. Chem.*, 2010, **79**, 1039–1046.
13 R. Begum, R. Rehan, Z. H. Farooqi, Z. Butt and S. Ashraf, *J. Nanopart. Res.*, 2016, **18**, 231.
14 K. Naseem, R. Begum and Z. H. Farooqi, *Environ. Sci. Pollut. Res.*, 2017, **24**, 6446–6460.
15 C. Kästner and A. F. Thünemann, *Langmuir*, 2016, **32**, 7383–7391.
16 K. Zhang, J. M. Suh, J.-W. Choi, H. W. Jang, M. Shokouhimehr and R. S. Varma, *ACS Omega*, 2019, **4**, 483–495.
17 A. Wang, H. Yin, H. Lu, J. Xue, M. Ren and T. Jiang, *Langmuir*, 2009, **25**, 12736–12741.
18 S. N. Mithila, A. H. Reaz, F. Z. Farhana, M. J. Shiddiky and S. H. Firoz, *RSC Adv.*, 2024, **14**, 38605–38614.
19 S. Senapati, S. Srivastava, S. B. Singh and K. Biswas, *Cryst. Growth Des.*, 2010, **10**, 4068–4075.
20 A. Loiacono, F. Fioravanti, G. Bertossi, E. A. Franceschini and G. I. Lacconi, *Discovery Chem.*, 2025, **2**, 88.
21 H. Yang, Y. Wu, Z. Zhuang, Y. Li and C. Chen, *Chin. J. Chem.*, 2022, **40**, 515–523.
22 A. Bhattacharjee and M. Ahmaruzzaman, *RSC Adv.*, 2016, **6**, 41348–41363.
23 G. B. Darband, M. Aliofkhazraei and A. S. Rouhaghdam, *Int. J. Hydrogen Energy*, 2017, **42**, 14560–14565.
24 A. Serrà, S. Grau, C. Gimbert-Suriñach, J. Sort, J. Nogués and E. Vallés, *Appl. Catal., B*, 2017, **217**, 81–91.
25 F. Feng, C. Ma, S. Han, X. Ma, C. He, H. Zhang, W. Cao, X. Meng, J. Xia and L. Zhu, *Angew. Chem., Int. Ed.*, 2024, **63**, e202405173.
26 H. Ye, Q. Wang, M. Catalano, N. Lu, J. Vermeylen, M. J. Kim, Y. Liu, Y. Sun and X. Xia, *Nano Lett.*, 2016, **16**, 2812–2817.
27 Y. Lv, X. Mao, W. Gong, D. Wang, C. Chen, P. Liu, Y. Lin, G. Wang, H. Zhang and A. Du, *Sci. China Mater.*, 2022, **65**, 1252–1261.
28 Y. Du, C. Zhao, S. Li, T. Dai, X. Yang, Y. Zhu and Q. Shao, *Chem. Soc. Rev.*, 2025, **54**, 7706–7739.
29 X. Gong, Z. Li, A. S. Pattamatta, T. Wen and D. J. Srolovitz, *Commun. Mater.*, 2024, **5**, 157.
30 X. Yi, V. Celorrio, H. Zhang, N. Robertson and C. Kirk, *J. Mater. Chem. A*, 2023, **11**, 22275–22287.
31 J. Hu, S. Li, Y. Li, J. Wang, Y. Du, Z. Li, X. Han, J. Sun and P. Xu, *J. Mater. Chem. A*, 2020, **8**, 23323–23329.
32 X. Zhang, H. Yin, X. Cheng, Z. Jiang, X. Zhao and A. Wang, *Appl. Surf. Sci.*, 2006, **252**, 8067–8072.
33 D. S. Sidhaye, T. Bala, S. Srinath, H. Srikanth, P. Poddar, M. Sastry and B. Prasad, *J. Phys. Chem. C*, 2009, **113**, 3426–3429.
34 W. Xu, K. Y. Liew, H. Liu, T. Huang, C. Sun and Y. Zhao, *Mater. Lett.*, 2008, **62**, 2571–2573.
35 K. H. Kim, Y. B. Lee, S. G. Lee, H. Park and S. S. Park, *Mater. Sci. Eng., A*, 2004, **381**, 337–342.
36 A. Nandi, M. DuttaGupta and A. Banthia, *Mater. Lett.*, 2002, **52**, 203–205.
37 H. Duan, D. Wang and Y. Li, *Chem. Soc. Rev.*, 2015, **44**, 5778–5792.
38 E. L. Smith, A. P. Abbott and K. S. Ryder, *Chem. Rev.*, 2014, **114**, 11060–11082.
39 P. C. Gomes-Junior, G. P. Longatto, K. K. de Lima Augusto, J. da Silveira Rocha, E. Piccin and O. Fatibello-Filho, *Microchim. Acta*, 2024, **191**, 425.
40 S. Datta, J. Mahin, E. Liberti, I. Manasi, K. J. Edler and L. Torrente-Murciano, *ACS Sustainable Chem. Eng.*, 2023, **11**, 10242–10251.
41 O. S. Hammond, K. J. Edler, D. T. Bowron and L. Torrente-Murciano, *Nat. Commun.*, 2017, **8**, 14150.
42 X. Meng, K. Ballerat-Busserolles, P. Husson and J.-M. Andanson, *New J. Chem.*, 2016, **40**, 4492–4499.
43 S. Datta, C. Jo, M. De Volder and L. Torrente-Murciano, *ACS Appl. Mater. Interfaces*, 2020, **12**, 18803–18812.

44 M. Espino, M. de los Ángeles Fernández, F. J. Gomez and M. F. Silva, *TrAC, Trends Anal. Chem.*, 2016, **76**, 126–136.
45 Y. Nahar and S. C. Thickett, *Polymers*, 2021, **13**, 447.
46 A. P. Abbott, D. Boothby, G. Capper, D. L. Davies and R. K. Rasheed, *J. Am. Chem. Soc.*, 2004, **126**, 9142–9147.
47 J. Y. Choi, Y. K. Lee, S. M. Yoon, H. C. Lee, B. K. Kim, J. M. Kim, K. M. Kim and J. H. Lee, *J. Am. Ceram. Soc.*, 2005, **88**, 3020–3023.
48 M. S. Che Zain, J. X. Yeoh, S. Y. Lee and K. Shaari, *Sustainability*, 2021, **13**, 12981.
49 A. Abbott, G. Frisch, S. Gurman, A. Hillman, J. Hartley, F. Holyoak and K. Ryder, *Chem. Commun.*, 2011, **47**, 10031–10033.
50 S. Sáringer, P. Rouster and I. Szilagyi, *J. Colloid Interface Sci.*, 2021, **590**, 28–37.
51 D. Lundqvist, *Arkiv for Kemi, Mineralogi Och Geologi*, 1947, **24**, 12.
52 Y. Li, Y. Cao and D. Jia, *J. Nanopart. Res.*, 2018, **20**, 1–8.
53 M. S. Bakshi, *Cryst. Growth Des.*, 2016, **16**, 1104–1133.
54 Y. Khan, S. Durrani, M. Mehmood, A. Jan and M. A. Abbasi, *Mater. Chem. Phys.*, 2011, **130**, 1169–1174.
55 L. Wang, M. Zhang and S. A. Redfern, *Clays Clay Miner.*, 2003, **51**, 439–444.
56 S. Bagheri, K. Shameli and S. B. Abd Hamid, *J. Chem.*, 2013, **2013**, 848205.
57 H. Shekaari, M. T. Zafarani-Moattar, A. Shayanfar and M. Mokhtarpour, *J. Mol. Liq.*, 2018, **249**, 1222–1235.
58 T. B. Pushpa, J. Vijayaraghavan, S. S. Basha, V. Sekaran, K. Vijayaraghavan and J. Jegan, *Ecotoxicol. Environ. Saf.*, 2015, **118**, 177–182.
59 K.-I. Sotowa, T. Amamoto, A. Sobana, K. Kusakabe and T. Imato, *Diamond Relat. Mater.*, 2004, **13**, 145–150.
60 M. Menelaou, K. Georgoula, K. Simeonidis and C. Dendrinou-Samara, *Dalton Trans.*, 2014, **43**, 3626–3636.
61 O. Ejeromedoghene, J. I. Orege, O. Oderinde, C. O. Okoye, M. Alowakennu, M. O. Nnyia and G. Fu, *Eur. Polym. J.*, 2022, **181**, 111711.
62 M. Francisco, A. van den Bruinhorst and M. C. Kroon, *Angew. Chem., Int. Ed.*, 2013, **52**, 3074–3085.
63 J. Gao, F. Guan, Y. Zhao, W. Yang, Y. Ma, X. Lu, J. Hou and J. Kang, *Mater. Chem. Phys.*, 2001, **71**, 215–219.
64 G. Gygli, X. Xu and J. Pleiss, *Sci. Rep.*, 2020, **10**, 21395.
65 A. P. Abbott, G. Capper, D. L. Davies, R. K. Rasheed and V. Tambyrajah, *Chem. Commun.*, 2003, 70–71.
66 A. P. Abbott, *ChemPhysChem*, 2005, **6**, 2502–2505.
67 A. P. Abbott, *ChemPhysChem*, 2004, **5**, 1242–1246.
68 K. M. Udert, T. A. Larsen, M. Biebow and W. Gujer, *Water Res.*, 2003, **37**, 2571–2582.
69 S. Kettaf, O. Guellati, A. Harat, H. Kennaz, D. Momodu, J. Dangbegnon, N. Manyala and M. Guerioune, *SN Appl. Sci.*, 2019, **1**, 34.
70 M. Li and G. Chen, *Nanoscale*, 2013, **5**, 11919–11927.
71 F. Bao, F. Tan, W. Wang, X. Qiao and J. Chen, *RSC Adv.*, 2017, **7**, 14283–14289.
72 Y. Kumar, S. Rani, J. Shabir and L. S. Kumar, *ACS Omega*, 2020, **5**, 13250–13258.
73 M. Kosmulski, *Adv. Colloid Interface Sci.*, 2020, **275**, 102064.
74 A. Chinnappan, S. K. Eshkalak, C. Baskar, M. Khatibzadeh, E. Kowsari and S. Ramakrishna, *Nanoscale Adv.*, 2019, **1**, 305–313.
75 D. Mohan and C. U. Pittman Jr, *J. Hazard. Mater.*, 2007, **142**, 1–53.
76 J. Sun, Y. Fu, G. He, X. Sun and X. Wang, *Catal. Sci. Technol.*, 2014, **4**, 1742–1748.
77 D. Shao, Q. Wang, X. Yao, Y. Zhou and X.-Y. Yu, *J. Mater. Chem. A*, 2022, **10**, 21848–21855.
78 F. Zhang, S. Zhao, K. Jin, H. Bei, D. Popov, C. Park, J. C. Neuefeind, W. J. Weber and Y. Zhang, *Appl. Phys. Lett.*, 2017, **110**, 011902.
79 C. Zhang, J. Yang, Y. Liu, Y. Li, Z. Dai, M. Han and J. Bao, *ChemistrySelect*, 2019, **4**, 42–48.